ACS Catalysis

Research Article

pubs.acs.org/acscatalysis

Hydrogen from Formic Acid via Its Selective Disproportionation over Nanodomain-Modified Zeolites

Ruth I. J. Amos,[*,†,§,⊥,∥] Falk Heinroth,[†] Bun Chan,[*,†,⊥] Antony J. Ward,[†] Sisi Zheng,[‡] Brian S. Haynes,[‡] Christopher J. Easton,[§,⊥,∥] Anthony F. Masters,[*,†] Thomas Maschmeyer,[*,†] and Leo Radom[*,†,⊥]

[†]School of Chemistry, The University of Sydney, Sydney, New South Wales 2006, Australia

[§]CSIRO Energy Transformed Cluster on Biofuels [⊥]ARC Centre of Excellence for Free Radical Chemistry and Biotechnology

[∥]Research School of Chemistry, Australian National University, Canberra, Australian Capital Territory 0200, Australia

[‡]School of Chemical and Biomolecular Engineering, The University of Sydney, Sydney, New South Wales 2006, Australia

Supporting Information

ABSTRACT: Sodium germanate is a nontransition-metal catalyst that is active in the selective dehydrogenation of formic acid. However, bulk sodium germanate has a very low surface area, limiting the availability of the germanate sites for catalysis. The dispersion of germanate in the zeolite ZSM-5 has been investigated both computationally and experimentally as a method for the provision of greater surface area and, therefore, higher activity per germanate site. Nanodomain islets of germanate dispersed in the germanium ZSM-5 zeolite invert selectivity from dehydration (in ZSM-5) to dehydrogenation of formic acid, potentially making Na-Ge-ZSM-5 a cost-effective catalyst for releasing hydrogen from formic acid.

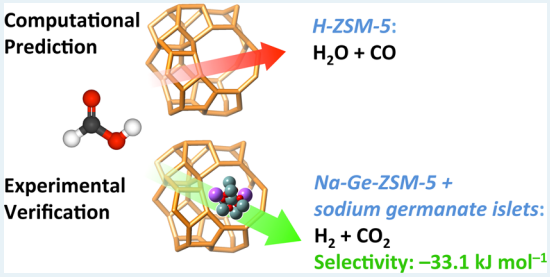

KEYWORDS: *zeolites, sodium germanate, formic acid, dehydration, dehydrogenation, hydrogen production*

INTRODUCTION

Clean energy alternatives are a major goal of research in the 21st century because the supply of fossil fuel is inherently limited. Hydrogen, for example, as used in fuel cells or direct combustion, is one possibility;[1] however, many difficulties still need to be overcome for the practical production, storage, and handling of hydrogen. In this context, formic acid is a renewable bioresource and possible source and reservoir of hydrogen that is safe to use, not flammable, nontoxic, and has a relatively high energy density.[2] The possible decomposition pathways of formic acid include dehydrogenation, producing H_2 plus CO_2

$$HCOOH \rightarrow H_2 + CO_2 \quad (1)$$

and dehydration, yielding H_2O plus CO.

$$HCOOH \rightarrow H_2O + CO \quad (2)$$

A catalyst promoting the selective dehydrogenation of formic acid would permit its use in the transport and storage of H_2. In a previous study, we found that sodium germanate is an excellent nontransition-metal catalyst for such a selective dehydrogenation of formic acid.[3] However, a bulk germanate catalyst suffers from its very low surface area, and therefore, the majority of the germanium in the catalyst is not available for catalysis. Zeolites are well-known high-surface-area solids that have been utilized for a wide variety of catalytic and noncatalytic applications.[4,5] In the present study, we investigate dispersion of germanate sites in zeolite ZSM-5 as a method for increasing the surface area of the sodium germanate catalyst. In our previous study, sodium germanate and H-silicalite-1 were investigated by both computational and experimental means.[3] This methodology has also been employed here, yielding powerful insights.

Zeolites, such as ZSM-5, contain a framework of SiO_4 tetrahedra with embedded trivalent aluminum in tetrahedral positions (AlO_4^- tetrahedra) and, therefore, have a negative framework charge, balanced by a counterion, the most common being Na^+ or H^+. Zeolites can be modified by exchanging these counterions for other cations, such as Li^+, Mg^{2+}, and Ca^{2+}.[6,7] In addition, a range of methods has been reported for their further modification by framework substitution, replacing Si with elements such as Ge[8−11] and Ga.[12−14] Successful framework substitution would effectively provide atomic dispersion of the substituent.

Zeolite structure and reactivity have been studied extensively.[5,15−17] Both computational and experimental investigations show that zeolites can act as formic acid dehydrogenation (with low selectivity) and dehydration catalysts.[18−20] In the present computational investigation, the zeolite active site of ZSM-5 was modified using a variety of counterions (i.e. H^+, Na^+, K^+, Li^+, Mg^{2+} and Ca^{2+}) and also modified to include germanium, gallium, or nitrogen as the framework substituents,

Received: October 29, 2014
Revised: May 25, 2015
Published: June 18, 2015

© 2015 American Chemical Society

DOI: 10.1021/cs501677b
ACS Catal. 2015, 5, 4353−4362

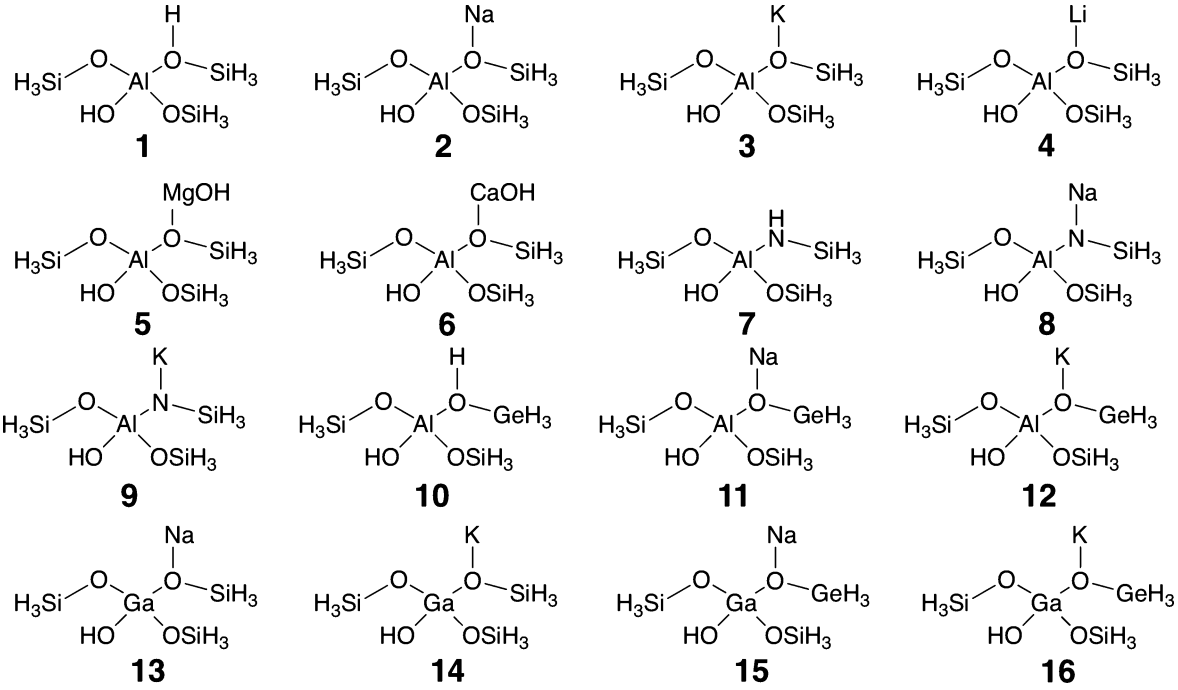

Figure 1. Structures of the zeolite models examined.

and calculations carried out to predict the consequent change in behavior toward formic acid decomposition.

The computational approach allows a broad range of zeolitic structures to be examined and deep insights into their behavior to be developed. The most promising germanium-containing ZSM-5 zeolites identified computationally were synthesized and catalytically evaluated for their ability to selectively dehydrogenate formic acid.

RESULTS AND DISCUSSION

Computational. Calculations were performed using the Gaussian09 program at the M06-2X/6-311+G(3df,2p)//BHandH-LYP/6-31+G(d,p) level of theory.[21]

To systematically investigate the effect of various chemical modifications on the reactivity of the active site of ZSM-5, a wide range of zeolite catalytic site models made up of clusters of four tetrahedral atoms (4T clusters) has been chosen to represent our principal substrates (Figure 1). Each zeolite model is a fragment of a structure based on ZSM-5, in which the catalytic site is modified. The modifications include replacing the proton in the active site of H-ZSM-5 (**1**) with a variety of alkali and alkaline-earth metal cations (**2**−**6**) and various combinations of these changes with other modifications that include exchanging an O atom with an alternative electronegative group−nitrogen (**7**−**9**), an Si atom with Ge (**10**−**12**), and the central Al atom with Ga (**13**−**16**).

The general reaction pathway involves the initial formation of a complex of formic acid with the catalyst site (formic acid···zeolite complex), a transition structure (TS), and a complex between the products and the catalyst (product···zeolite complex), consistent with previous studies of the germanate and silicalite structures[3] and also studies of zeolite-type catalysts used for other processes[22] (Figure 2). Formic acid exists as two major conformational isomers − cis and trans (with respect to the hydrogen atoms). In all cases, the trans formic acid-zeolite complex is lower in energy than the cis and is also lower in energy than the separate reactants (see Supporting Information for a full description). To undergo dehydrogenation, the formic acid needs to rotate from the trans to the cis conformation. The barrier predicted for rotation of free formic acid is 46.7 kJ mol^{-1}, and the cis conformer of formic acid is calculated to be 17.2 kJ mol^{-1} higher in energy than the trans conformer. Formic acid at room temperature exists as a dimer;[23−25] however, it is estimated that the mole fraction of dimeric formic acid is 0.001 at 600 K,[25] and a similarly low fraction is expected to be present under the reaction conditions of this experiment (300 °C or 573 K). Therefore, monomeric formic acid is modeled in our calculations.

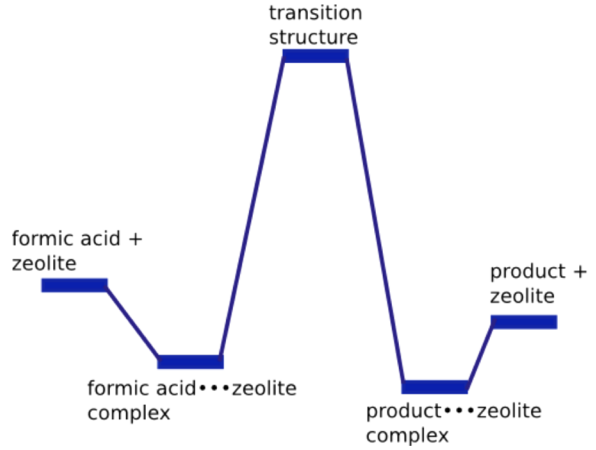

Figure 2. General potential energy diagram for the zeolite-catalyzed dehydrogenation or dehydration of formic acid.

The computed gas-phase free energy barriers ($\Delta G^{\ddagger}$) for dehydrogenation and dehydration in Table 1 are calculated as energy differences measured from the trans formic acid···zeolite complex. Also included in Table 1 are the energy selectivities ($\Delta\Delta G^{\ddagger}$), defined here as the difference in the free energy barriers for dehydrogenation and dehydration. The desired preference for dehydrogenation corresponds to a negative value

DOI: 10.1021/cs501677b
ACS Catal. 2015, 5, 4353−4362

Table 1. Calculated Gas-Phase Free Energy Barriers ($\Delta G^{\ddagger}$, kJ mol^{-1}) and Energy Selectivities ($\Delta\Delta G^{\ddagger}$, kJ mol^{-1}) for Catalyst Models in Figure 1[a]

structure no. (modification)	$\Delta G^{\ddagger}$ H_2/CO_2	$\Delta G^{\ddagger}$ H_2O/CO	energy selectivity[b]
no catalyst	292.6	293.3	−0.7
aluminum catalysts			
1 (H-ZSM-5)	199.0	158.6	40.4
2 (Na)	187.3	218.5	−31.2
3 (K)	181.8	216.9	−35.0
4 (Li)	213.1	204.5	+8.6
5 (Mg)	232.5	176.6	+55.9
6 (Ca)	230.3	196.0	+34.4
nitrogen catalysts			
7 (N)[c]	184.3	192.0	−7.7
8 (NaN)	185.3	179.9	+5.4
9 (KN)	169.1	173.6	−4.5
germanium catalysts			
10 (HGe)[c]	163.6	133.8	+29.8
11 (NaGe)	183.5	216.5	−33.1
12 (KGe)	157.4	222.7	−65.4
gallium catalysts			
13 (NaGa)	185.1	215.6	−30.5
14 (KGa)	182.7	216.7	−34.0
15 (NaGaGe)	159.9	178.7	−18.8
16 (KGaGe)	175.2	200.7	−25.5

[a]The structure numbers relate to the models in Figure 1. An abbreviated description of the modification to H-ZSM-5 is presented in parentheses. [b]A negative value for the reaction selectivity indicates a preference (i.e., lower barrier) for dehydrogenation. [c]Effective barriers that incorporate an energy of 80.3 kJ mol^{-1} for **7** and 34.6 kJ mol^{-1} for **10** for proton exchange from the lowest energy isomer to the active catalytic form. The barriers starting from the catalytically active form are 104.0 and 111.7 kJ mol^{-1} for **7** and 128.9 and 99.1 kJ mol^{-1} for **10** for dehydrogenation and dehydration, respectively.

for $\Delta\Delta G^{\ddagger}$. Representative transition structures are shown in Figure 3, and full catalytic cycles for the sodiated catalyst are shown in Figure 4.

The uncatalyzed barrier for dehydrogenation of formic acid is predicted to be 292.6 kJ mol^{-1} (Table 1). The calculated dehydration barrier is approximately equal to the dehydrogenation barrier (Table 1); therefore, a catalyst is necessary to lower barrier heights selectively and, consequently, to discriminate toward dehydrogenation selectivity.

Our calculations predict that the barrier for dehydrogenation in the standard ZSM-5 zeolite (**1**, H-ZSM-5 model) is 199.0 kJ mol^{-1} (Table 1). The same catalyst has a calculated barrier to dehydration of 158.6 kJ mol^{-1} (Table 1). Because the dehydration barrier is much lower than that for dehydrogenation, it is predicted computationally that the active site of H-ZSM-5 (**1**) would selectively produce H_2O and CO in formic acid decomposition.

Changing the counterion from a proton to a sodium or potassium ion (**2** or **3**, Figure 1) is predicted to change the energy selectivity such that hydrogen and carbon dioxide are the preferred products (Table 1). However, a lithium counterion does not lead to selective dehydrogenation, and replacing the proton in H-ZSM-5 with an alkaline-earth metal ion such as Ca or Mg (**5** or **6**, Figure 1) is also not predicted to lead to selective dehydrogenation (Table 1). Further calculations aimed at rationalizing this behavior are in progress.

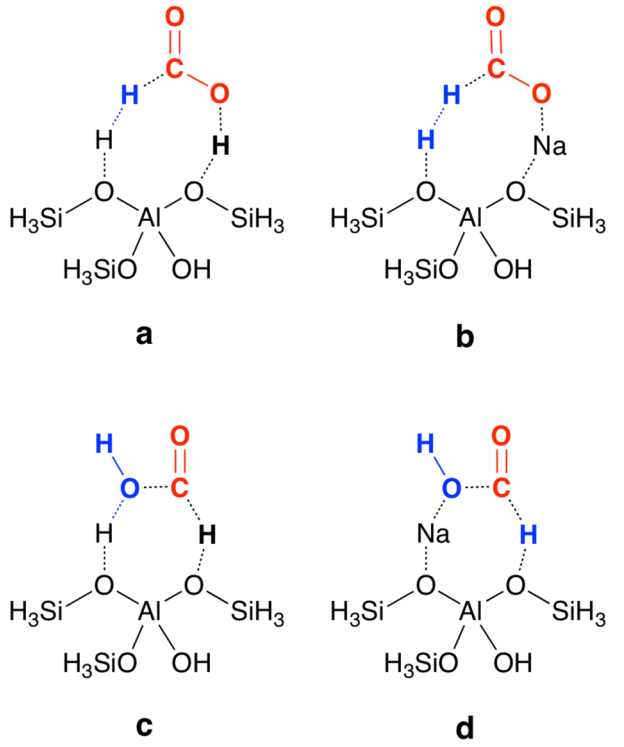

Figure 3. Representative transition structures for (a) dehydrogenation using H-ZSM-5 (1), (b) dehydrogenation using Na-ZSM-5 (2), (c) dehydration using H-ZSM-5 (1), and (d) dehydration using Na-ZSM-5 (2). The formic acid reagent is shown in bold; products CO_2 and CO, red; and H_2 and H_2O, blue. See Figure 4 for the complete catalytic cycles for b and d.

Changing one oxygen atom in the active site to a nitrogen atom (**7**–**9**, Figure 1) has the effect of reducing the energy selectivity to near zero, regardless of whether the counterion is a proton, a sodium ion, or a potassium ion (Table 1).

The incorporation of both sodium and germanium (**11**, Figure 1) is predicted to give selective dehydrogenation with a slightly lower barrier to reaction than that of Na-ZSM-5 (**2**) (Table 1). This is an anticipated result, given our calculations on the bulk sodium germanate.[3] Na-Ge-ZSM-5 (**11**) is a model for atomic dispersion of sodium germanate in a zeolite and is predicted to have a barrier and selectivity for dehydrogenation similar to that of the bulk germanate[3] ($\Delta G^{\ddagger}$ = 183.5 kJ mol^{-1} for **11** vs 176.8 kJ mol^{-1} for the sodiated tetrahedral germanate model,[3] and $\Delta\Delta G^{\ddagger}$ = −33.1 kJ mol^{-1} for **11** vs −32.1 kJ mol^{-1} for the sodiated tetrahedral germanate model[3]), making this zeolite an attractive synthetic target.

The improved energy selectivity given by the potassium ion (**3**, Figure 1) in conjunction with the lower activation energy given by germanium incorporation was computationally investigated to see if the trend of lower barriers and greater energy selectivity could be extended. The combined potassium–germanium analogue (**12**, Figure 1) is, indeed, predicted to produce excellent energy selectivity for dehydrogenation (−65.4 kJ mol^{-1}, Table 1), and to have a lower dehydrogenation barrier than that for the sodium–germanium derivative: 157.4 kJ mol^{-1} (K-Ge-ZSM-5) vs 183.5 kJ mol^{-1} (Na-Ge-ZSM-5).

Several other combinations of substituents were also found to be selective for dehydrogenation. These include the combined sodium–gallium analogue, **13**, and the potassium–

DOI: 10.1021/cs501677b
ACS Catal. 2015, 5, 4353–4362

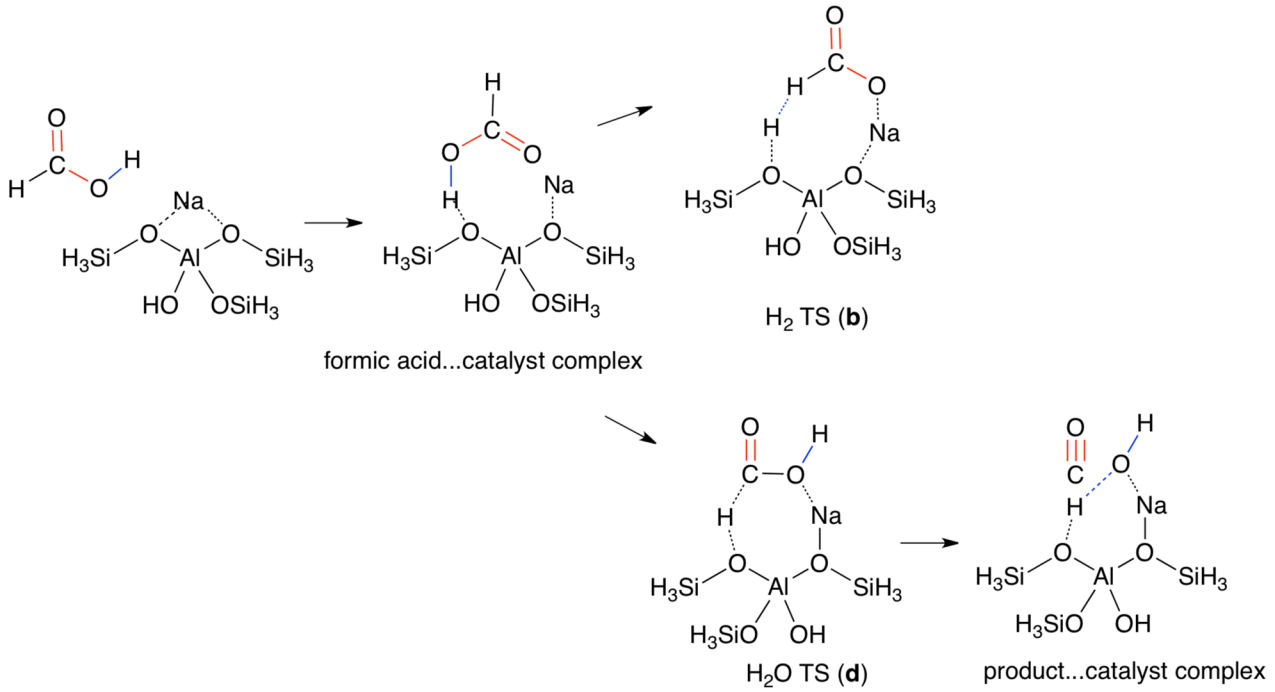

Figure 4. Complete catalytic cycles for the sodiated catalyst (**2**).

gallium catalyst, **14**, with energy selectivities of −30.5, and −34.0 kJ mol^{-1}, respectively. The inclusion of both germanium and gallium substituents lowers barriers to dehydration, which is not desirable. The combined sodium-gallium-germanium catalyst (**15**) has a barrier to dehydrogenation that is similar to that of the potassium-germanium catalyst but does not have the degree of energy selectivity of the sodium- or potassium-germanium analogues (**11** and **12**) (Table 1). Similarly, the combined potassium-gallium-germanium catalyst (**16**) does not have the degree of energy selectivity of the potassium-germanium analogue (**12**) (Table 1).

The sodium-germanium zeolite (**11**) and potassium-germanium zeolite (**12**) are predicted to be selective and to have moderately low barriers for hydrogen production. Accordingly, these two catalysts were synthesized and tested for dehydrogenation activity.

Synthesis and Characterization. To follow up on the predictions of the computational investigation, a selection of the proposed modified zeolites was synthesized according to literature protocols[9] and subsequently tested for catalytic activity in the decomposition of formic acid. The experimental systems include the protonated and sodiated ZSM-5 (based on catalyst models **1** and **2**) as well as the germanium analogues: H-Ge-ZSM-5 (based on catalyst model **10**), Na-Ge-ZSM-5 (based on catalyst model **11**), and K-Ge-ZSM-5 (based on catalyst model **12**). The protonated and potassium analogues of the zeolite catalysts were synthesized by ion-exchange of the sodiated catalyst with the appropriate ion (NH_3 and KNO_3 are used to make the protonated and potassium catalysts, respectively; see experimental section for details).

Figure 5 displays examples of X-ray diffraction (XRD) patterns for H-ZSM-5, Na-ZSM-5, H-Ge-ZSM-5, and Na-Ge-ZSM-5 zeolites. The diffraction patterns of all the zeolite samples can be indexed in the monoclinic MFI crystal structure and are in good agreement with that reported for ZSM-5.[8,9] The corresponding lattice constants can be found in Table S4 of the Supporting Information. As reported elsewhere, the

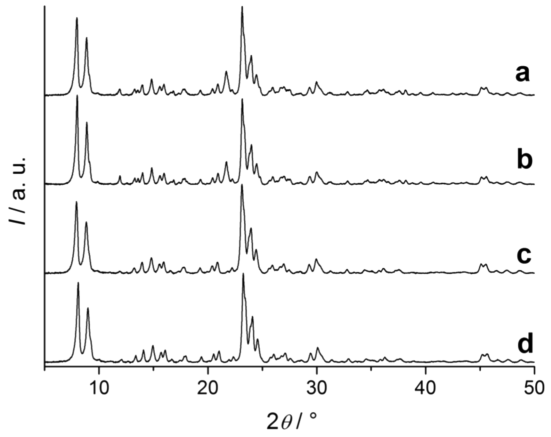

Figure 5. XRD patterns of (a) H-Ge-ZSM-5, (b) Na-Ge-ZSM-5, (c) H-ZSM-5, and (d) Na-ZSM-5.

lattice dimensions appear to be relatively insensitive toward the molar composition of the zeolites.[8] The XRD measurements of the germanium zeolites were taken on samples that were not washed with sodium nitrate and show a reflection at ∼22° that is consistent with the presence of germanate islets in the sample. Apart from this impurity, the samples are deemed to consist of pure-phase materials.

Nitrogen sorption measurements were performed, and the calculated structural parameters for all the zeolite catalysts examined are listed in Table 2. In addition, selected isotherms are presented in Figure 6. For all the zeolitic samples, the nitrogen adsorption isotherms can be described as standard Type I curves, characterized by an initial sharp increase and leveling off at a very low relative pressure of <0.01, typical for microporosity (Figure 6). Bulk germanate samples, however, have very little surface area (Table 2). It can be seen from the adsorption curves that the wash with sodium nitrate increases the volume of the zeolite (Figure 6, Table 2).

DOI: 10.1021/cs501677b
ACS Catal. 2015, 5, 4353−4362

Table 2. Molar Compositions and Structural Parameters for the Catalysts

sample	S_{BET}, $m^2\ g^{-1}$	$S_{t\text{-}plot}$, $m^2\ g^{-1}$	V_{pore}, m^3	$V_{t\text{-}plot}$, m^3	Si/Al	Si/Ge	Si/Na	Si/K
Na-ZSM-5	359	220	0.26	0.10	24:1		21:1	
H-ZSM-5	393	223	0.25	0.12	23:1		120:1	
Na-Ge-ZSM-5	279	227	0.15	0.11	26:1	4:1	10:1	
Na-Ge-ZSM-5[a]	380	288	0.21	0.14	23:1	8:1	12:1	
H-Ge-ZSM-5	357	238	0.19	0.09	30:1	12:1	14:1	
K-Ge-ZSM-5	276	201	0.16	0.09	26:1	9:1	36:1	13:1
K-Ge-ZSM-5[a]	353	267	0.2	0.13	24:1	12:1	48:1	24:1
					Si/Ge	Al/Ge	Na/Ge	
sodium aluminogermanate	3.17	3.49	0.00014	0.000099	1:27	1:27	1:3	
sodium germanate[b]							1:3	
Na-Ge-silicalite	280	140	0.15	0.069	9:1		1:3	

[a]Washed with aqueous $NaNO_3$; see the Experimental Section for details. [b]See ref 3.

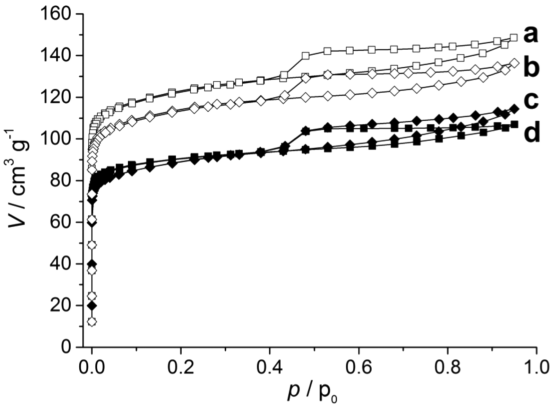

Figure 6. Nitrogen sorption measurements at 77 K for (a) Na-Ge-ZSM-5 and (b) K-Ge-ZSM-5 samples after washing with $NaNO_3$, and (c) K-Ge-ZSM-5 and (d) Na-Ge-ZSM-5 samples as-synthesized.

To determine the molar compositions of the zeolites synthesized, elemental analyses using ICP−AES were performed, and the ratios obtained are included in Table 2. The zeolites exhibit a Si/Al ratio of ~25:1, which is consistent with the molar composition of 20:1 of the reaction mixture.

The Si/Ge ratio of the Na-Ge-ZSM-5 samples is 4:1, a higher level of germanium than that of the reaction mixture (the Si/Ge ratio in the reaction mixture is 10:1). There is also a large discrepancy in the Al/Na ratios between Na-ZSM-5 and Na-Ge-ZSM-5, with ratios of 1:1.1 and 1:2.6, respectively. A 1:1 ratio is expected for the sodiated catalysts because the sodium is a counterion to the negatively charged AlO_4^- group in the zeolite framework. The concentration of both germanium and sodium in the sample points to the formation of sodium germanate in the catalyst. Once washed with $NaNO_3$ (see the Experimental Section for details), the Si/Ge ratio in the Na-Ge-ZSM-5 catalyst changes to 8:1, which is more consistent with the composition of the reaction mixture. The sodium nitrate-washed Na-Ge-ZSM-5 catalyst also has a lower level of sodium (1:1.9 Al/Na). The sodium nitrate wash therefore removes sodium germanate from the catalyst. The slightly elevated levels of sodium and germanium remaining (compared with the 1:1, Al/Na ratio and the 10:1 Si/Ge ratio expected) indicate that the sodium germanate has not been completely washed out of the sample (Table 2).

The potassiated catalyst was synthesized by performing ion exchange with potassium nitrate solution on the Na-Ge-ZSM-5 catalyst. The Na/Al ratio in the potassiated catalyst was 1.4:1, a level similar to the sodium nitrate-washed Na-Ge-ZSM-5 and higher than was expected because potassium is the expected counterion in this case (Table 2). However, the differences in the Na/Al ratio from the Na-Ge-ZSM-5 catalyst (2.6:1 for Na-Ge-ZSM-5 down to 1.4:1 for K-Ge-ZSM-5)) and the Si/Ge ratio (4:1 for Na-Ge-ZSM-5 to 9:1 for K-Ge-ZSM-5) show that the potassium nitrate wash has removed some of the sodium germanate present in the original Na-Ge-ZSM-5 zeolite. Interestingly, the K/Al ratio is 0.5:1, indicating that both sodium and potassium ions are acting as counterions to the framework negative charge.

The ion-exchange procedures were also performed on the sodiated germanium catalyst after it had been washed with $NaNO_3$ to give a washed version of the potassiated germanium zeolite. This washed version has even less germanium and sodium than the purely ion-exchanged version: the Ge/Al ratio in the washed zeolite is 2:1, and Na/Al is 0.5:1, whereas the K/Al ratio is now 1:1, as expected when K^+ is the counterion (Table 2). We note that the surface areas of the M-Ge-ZSM-5 (M = Na, K) are less than those of X-ZSM-5 (X = Na, H) and that the proportions of germanium in M-Ge-ZSM-5 are reduced by washing with aqueous $NaNO_3$, consistent with the presence of alkali metal germanates on the zeolite surface. The catalytic results are interpreted in terms of the germanium being present as germanate islets on the surface. A measure of the proportions of this dispersed germanium is provided by normalizing the activity to the germanium content (see below).

To confirm that Ge was present in the MFI structure, infrared (FTIR) and Raman spectra were recorded. The FTIR spectra (Figure 7A) exhibit well-defined absorptions at 450, 800, and 1220 cm^{-1}, which can be assigned as tetrahedral T−O−T (Si−O−Si, Si−O−Al, Si−O−Ge) deformations as well as symmetric and asymmetric stretching vibrational modes.[8,18,26,27] A well-defined absorption at 550 cm^{-1} can be attributed to the double-five-membered rings in the MFI structure. Additional evidence for Ge incorporation is an absorption at 1030 cm^{-1} (assigned to the Si−O−Ge asymmetric stretch[27]), present in the Ge-ZSM-5 samples, whereas the samples without germanium have an absorption at 1100 cm^{-1}. As reported in the literature, the intensities of the absorptions at 550, 800, and 1100 cm^{-1} decrease with increasing incorporation of Ge in the framework due to the slight changes in the T−O distances and T−O−T angles.[8,26,25]

Calculated vibrational frequencies using 28T models (described in the Supporting Information) also provide support for this difference in absorptions, with an absorption at 1050 cm^{-1} found in the Na-ZSM-5 model shifted to 972 cm^{-1} in the Na-Ge-ZSM-5 model. Similarly, an absorption at 1100 cm^{-1} in

DOI: 10.1021/cs501677b
ACS Catal. 2015, 5, 4353−4362

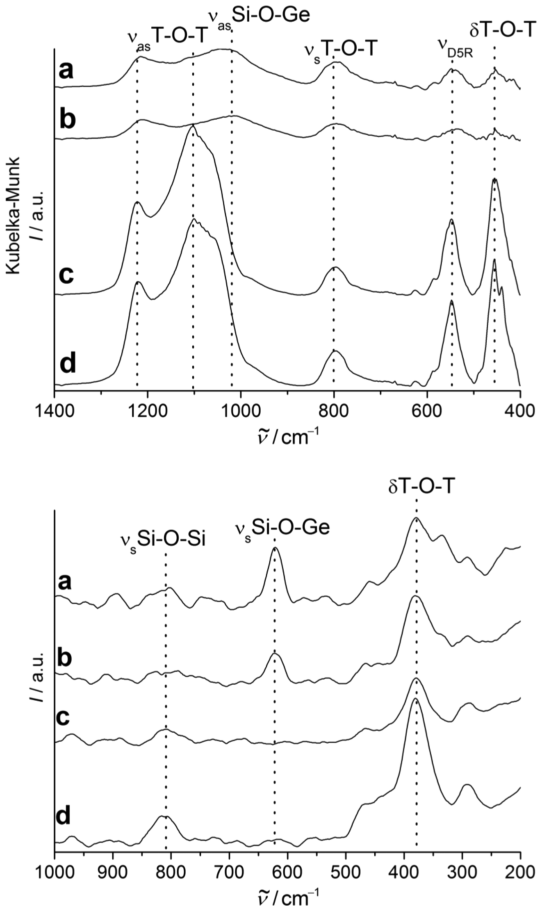

Figure 7. FTIR spectra (top) and Raman spectra (bottom) of (a) H-Ge-ZSM-5, (b) Na-Ge-ZSM-5, (c) H-ZSM-5, and (d) Na-ZSM-5.

the Na-ZSM-5 model shifts to 1050 cm^{-1} in the Na-Ge-ZSM-5 model. Both of these absorptions relate to Si−O−Ge/Si or Si/Ge−O−Al stretches (see Supporting Information for details). A similar shift occurs in the protonated ZSM-5 28T model calculations in which the absorptions at 1115 and 1160 cm^{-1} with no Ge present shift to 1073 and 1130 cm^{-1} in the germanium catalyst model.

The Raman spectra recorded (Figure 7B) show absorptions at 350 to 400 cm^{-1}, typical of T−O−T deformation vibrations. Another absorption at 806 cm^{-1} can be assigned to Si−O−Si symmetric stretching vibration modes. In the Ge-containing ZSM-5 samples, an additional well-pronounced absorption at 622 cm^{-1} can be seen. The assignment of this absorption is supported by calculations on the 28T models that show a greater intensity absorption at 650 cm^{-1} for the H-Ge-ZSM-5 model and 644 and 663 cm^{-1} for the Na-Ge-ZSM-5 model when compared with the respective models without germanium (see the Supporting Information for details). These absorptions are associated with the Si−O−Ge stretching modes in the models, in agreement with the literature, which reports that an absorption in this region appears due to the presence of tetrahedrally coordinated Ge in the framework and can be assigned to an Si−O−Ge symmetric stretching vibration.[8]

Catalytic Activity. The catalytic performance was evaluated by passing argon, containing nominally 1 mol % formic acid vapor, over each of the catalysts in a furnace held at 300 °C. Under these conditions, formic acid exists essentially only in the monomeric form, as modeled in the calculations. Control experiments (in the absence of catalyst) revealed minimal loss of formic acid, irrespective of its passage over the quartz wool support used in the catalytic tests (Table 3). Under the catalytic test conditions, at least 50% of the formic acid is reacted. Apart from unreacted formic acid, the only products detected are CO, CO_2, and H_2. Comparing absolute concentrations, the yield of CO_2 in the products is within 5% of that of H_2, confirming that hydrogen production occurs as described by reaction 1. The results were not mass-transfer-limited (see Supporting Information for details). Each catalyst was tested at least two times on separate dates, with variations in relative product selectivity being <10%. After equilibration, time-on-stream gave a constant reading for 60 min (see the Supporting Information for details). Table 3 summarizes the results in terms of the apparent selectivity toward dehydrogenation, evaluated as the ratio, in the products, of the concentration of H_2 to the sum of the H_2 and CO concentrations. Table 3 also shows the concentration of hydrogen and carbon monoxide in parts per million and the concentrations normalized to the germanium content of each germanium catalyst.

The ZSM-5 catalyst synthesis leads to the sodiated catalyst Na-ZSM-5, which can then be converted to H-ZSM-5 through ion exchange with NH_3 followed by calcination. The decomposition of formic acid catalyzed by Na-ZSM-5 gives

Table 3. Gas Components Reported at Steady State (60 min at 300 °C) Expressed as Ratios and as Concentrations in the Gas Stream (ppm) and Normalized to Germanium Content (Ge norm) for Germanium Catalysts

entry	zeolite (computational model number)	selectivity,[a] %	H_2 (ppm)	CO (ppm)	H_2 Ge norm	CO Ge norm
A	blank	75	300	100		
B	Na-ZSM-5 (**2**)	27	2000	5500		
C	H-ZSM-5 (**1**)	21	1200	4500		
D	Na-Ge-ZSM-5 (**11**)	87	3900	600	219	34
E	Na-Ge-ZSM-5[b] (**11**)	19	700	3000	78	336
F	H-Ge-ZSM-5[b] (**10**)	20	1100	4400	157	629
G	sodium aluminogermanate	88	4200	600	58	8
H	K-Ge-ZSM-5 (**12**)	59	2900	2000	316	218
I	K-Ge-ZSM-5[b] (**12**)	16	800	4300	97	520
J	sodium germanate[c]	94	4900	300	64	4
K	protonated silicalite[c]	26	1500	4300		
L	Na-silicalite[c]	39	2500	3900		
M	Na-Ge-silicalite	69	3800	1800	464	220

[a] $(H_2/(H_2 + CO)) \times 100$. [b] Washed with aqueous $NaNO_3$; see above for details. [c] From ref 3.

DOI: 10.1021/cs501677b
ACS Catal. 2015, 5, 4353−4362

CO as the main product[28] but also gives CO_2 and H_2, with a selectivity for H_2 of 27% (Table 3, entry B), an outcome similar to that found in the literature.[29] The difference in barrier heights for dehydrogenation and dehydration for Na-ZSM-5 is calculated to be −31.2 kJ mol^{-1} (**2**, Table 1), leading to the expectation of dehydrogenation when using this catalyst; however, the barrier to dehydrogenation for Na-ZSM-5 is much higher (187.3 kJ mol^{-1}) than the barrier to dehydration using H-ZSM-5 (158.6 kJ mol^{-1}). Therefore, the high levels of carbon monoxide produced in the reaction over Na-ZSM-5 may be associated with small numbers of H-ZSM-5 sites in the catalyst. In addition, silanol defect sites in silicalite have been shown computationally and experimentally to selectively dehydrate formic acid,[3] and the presence of these sites in the Na-ZSM-5 catalyst would also lead to carbon monoxide production. After the ion exchange with NH_3, H-ZSM-5 preferentially dehydrates formic acid, with a lower dehydrogenation selectivity of 21% (Table 3, entry C). The latter result is in agreement with the calculations, which predict that dehydration is preferred when using H-ZSM-5 because the barrier for dehydration is 40.4 kJ mol^{-1} lower than that for dehydrogenation (Table 1, **1**).

The Na-Ge-ZSM-5 results in Table 3 have been normalized to the germanium content in the catalyst to probe whether utilizing a zeolite catalyst has improved the activity of the germanate catalyst. Na-Ge-ZSM-5 gives a lower selectivity overall than sodium germanate (87% compared with 94%, entries D and J);[3] however, the amount of H_2 produced when normalized to the amount of germanium in the catalyst is much higher (219 ppm for Na-Ge-ZSM-5 compared with 64 ppm for sodium germanate). Therefore, as per design, there is a much greater dispersion of germanium (albeit in the form of nanoislets, rather than atomically distributed), which has led to a great improvement of germanium utilization. Once the Na-Ge-ZSM-5 catalyst is washed with sodium nitrate, both the selectivity for hydrogen and the activity relative to germanium content are vastly decreased (19% and 78 ppm, respectively, Table 3, entry E), indicating that a sodium germanate-like substance is being washed out of the zeolite, in agreement with the ICP measurements (Table 2).

The synthesis of K-Ge-ZSM-5 involves ion exchange of Na-Ge-ZSM-5 with potassium nitrate. Reaction of formic acid over K-Ge-ZSM-5 gives results in agreement with the ICP results in Table 2, suggesting that the sodium germanate-like substance is washed out during the ion-exchange process; hence, the overall selectivity for dehydrogenation for K-Ge-ZSM-5 is lower (59% compared with 87% for the Na-Ge-ZSM-5; Table 3, entries H and D). However, when the results are normalized to the amount of germanium present in the catalyst, the K-Ge-ZSM-5 is more active in dehydrogenation than is Na-Ge-ZSM-5.

The greater dehydrogenation selectivity of K-Ge-ZSM-5 is supported by our calculations that predict that the dehydrogenation barrier for the potassium germanium catalyst is similar to the dehydration barrier for any protonated aluminum site in the catalyst (157.4 kJ mol^{-1} for K-Ge-ZSM-5 and 158.6 kJ mol^{-1} for H-ZSM-5), significantly promoting dehydrogenation in any potassium-containing active site. However, if a germanium atom is incorporated into a protonated active site in the catalyst, then the barrier to dehydration is predicted to be 133.8 kJ mol^{-1} (Table 1, **10**), leading to the high levels of dehydration that also occur with this catalyst. In addition, any silanol defects in the catalyst have been shown computationally and experimentally to promote dehydration,[3] and the removal of sodium germanate is thought to provide access to silanol defects, leading to carbon monoxide production. Therefore, although the K-Ge-ZSM-5 zeolites contain active sites with high dehydrogenation activity, as predicted by our computations, the activity of these sites is mitigated by the high dehydration activity of other sites (particularly silicalite defect sites and protonated germanium-containing sites) in the zeolite, confounding results and leading to higher levels of carbon monoxide production.

If a sodium nitrate wash is performed on Na-Ge-ZSM-5 followed by ion-exchange to form the K-Ge-ZSM-5 catalyst, then once again, the overall selectivity for hydrogen is reduced (Table 3, entry I). However, the dehydrogenation activity normalized to germanium is slightly higher than that for the sodium nitrate-washed Na-Ge-ZSM-5 (97 ppm for K-Ge-ZSM-5 vs 78 ppm for Na-Ge-ZSM-5; Table 3).

In an attempt to recreate the impurity that had been washed out of the Na-Ge-ZSM-5 catalyst, the synthesis protocol for Ge-ZSM-5 was followed using GeO_2 rather than silica while the other reagents were unchanged (see Experimental Section for details). The result was a silica-free, crystalline white powder; however, while being crystalline, this substance did not show the required monoclinic MFI crystal structure and was therefore not related to ZSM-5 in structure (Figure 8). Indeed,

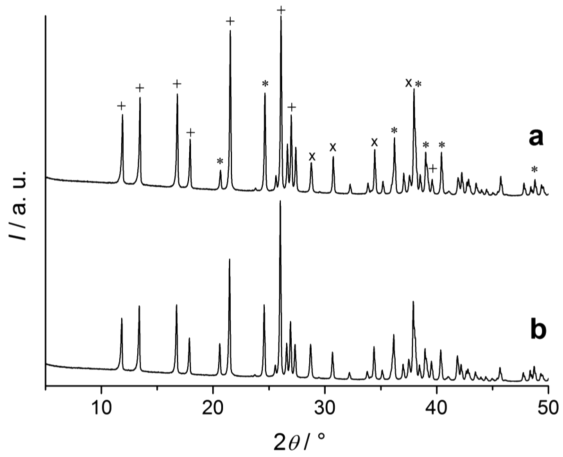

Figure 8. Measured X-ray diffraction pattern of synthesized sodium aluminogermanate (a) before and (b) after being utilized for catalysis: peaks assigned to octahedral units (+, $Na_4Ge_9O_{20}$), tetrahedral units (×, $Na_2Ge_4O_9$), and rutile germanium(IV) oxide (*).[30]

the X-ray diffraction pattern gives evidence that the silica-free substance is very similar to a sodium germanate (made up of two forms: $Na_4Ge_9O_{20}$ and $Na_2Ge_4O_9$).[3,30] Analysis after use shows a similar X-ray diffraction pattern (Figure 8), suggesting that the crystal structure of the aluminogermanate is not changed upon reaction with formic acid. The sodium aluminogermanate was not microporous in nature, as confirmed by nitrogen sorption analysis. ICP−AES analysis shows a Ge/Na ratio of 3:1 and an Al/Ge ratio of 1:27 (Table 2). Reaction of formic acid over this catalyst gives a selectivity for hydrogen of 88%, a result similar to that for the original Na-Ge-ZSM-5 (87%) (Table 3, entries G, D); therefore, we propose that this product is very similar in composition to the active component that is removed from Na-Ge-ZSM-5 when the catalyst is washed with $NaNO_3$. The results for this catalyst are also very similar to those for the reaction of formic acid over

DOI: 10.1021/cs501677b
ACS Catal. 2015, 5, 4353−4362

sodium germanate, for which the selectivity for H_2 under the same conditions was 94%.[3]

The catalysis results as well as the characterization of the zeolites and the sodium aluminogermanate indicate strongly that the sodium−germanium zeolite contains islets of bulk sodium germanate that can be removed by washing with sodium nitrate solution. The catalytic results from the germanium zeolites suggest that the presence of sodium germanate is necessary for the selective dehydrogenation of formic acid. The reactivity of the silicalite background and protonated aluminum sites in zeolites are dominating factors in the zeolite decomposition of formic acid. Although silicalite has no inbuilt active sites for reaction (such as the tetrahedral AlO_4^- sites in the zeolite), its reactivity is still high in the dehydration of formic acid (Table 3).[3] The reactivity of silicalite is thought to be due to defect sites in the framework of the catalyst that give catalytically active silanol (SiOH) groups.[3,11,31−36] However, the results from catalysis over unwashed Na-Ge-ZSM-5 suggest that enough bulk sodium germanate can be distributed in the germanium zeolite to block access to dehydrating silanol groups, leading to preferential dehydrogenation of formic acid.

Because it is the sodium germanate islets in the germanium zeolite that are performing the dehydrogenation catalysis, it is possible that the aluminum in the zeolite is not a necessary part of the catalyst. Accordingly, aluminum-free germanium MFI structures were synthesized to see if comparable germanate islets could be produced with dehydrogenation capabilities (see the Experimental Section for details). The aluminum-free analogue of the ZSM-5 (MFI type) zeolite is H-silicalite-1. H-Silicalite-1 and Na-silicalite-1 have previously been shown by both calculations and experiment to selectively dehydrate formic acid (Table 3).[3] In a manner similar to that of the creation of germanium zeolites, germanium(IV) oxide was added to the silicalite reaction mixture in the synthesis of the germanium silicalite (see the Experimental Section for details). The germanium−silicalite analogues were ion-exchanged in a manner analogous to the zeolite ion-exchange and similarly tested for dehydrogenation of formic acid.

The as-synthesized Na-Ge-silicalite was found to selectively dehydrogenate formic acid (Table 3, entry M), suggesting that sodium germanate was present in the silicalite from the synthesis procedure. ICP analysis of the silicalite (Table 2) also indicates the presence of germanate with a Si/Ge ratio of 9:1 and an Na/Si ratio of 1:27. The dehydrogenation activity for the Na-Ge-silicalite normalized to germanium is 464 ppm, higher than both Na-Ge-ZSM-5 (219 ppm) and K-Ge-ZSM-5 (316 ppm, Table 3). However, the dehydration activity for the silicalite is also high at 220 ppm normalized to germanium content, which is comparable to the 218 ppm for K-Ge-ZSM-5. These experimental results suggest that the germanium silicalite is also an effective carrier of sodium germanate islets. The operation of the catalysts and the chemistry at the germanate sites is consistent with the predictions of our calculations.

CONCLUSION

Bulk sodium germanate selectively dehydrogenates formic acid[3] but has a very low surface area as a result of its nonporous nature. Islets of sodium germanate can be distributed through a ZSM-5 zeolite or silicalite structure to give a dehydrogenation catalytic activity that is very similar to that of the bulk germanate but with a much higher activity level per germanium atom. The dehydration activity of silanol groups appears to be blocked by the presence of sodium germanate, and therefore, the dehydration activity is greatly reduced, allowing the use of a sodium-germanium zeolite, a potassium-germanium zeolite, or a sodium-germanium silicalite as a high-surface-area, selective dehydrogenation catalyst for formic acid. The K-Ge-ZSM-5 catalyst is more active in dehydrogenation than the Na-Ge-ZSM-5 when normalized to germanium content, in agreement with computational predictions.

EXPERIMENTAL SECTION

Theoretical Methods. Standard density functional theory calculations were performed with the Gaussian 09 program.[21]

There has been some discussion in the literature as to which model size is most appropriate for particular zeolite frameworks, with some computational studies showing that larger models are necessary for accuracy in calculations[3,37] and others finding that calculations on models with four tetrahedral atoms (4T) give results that are very similar to the larger 28T models.[22] It would thus seem that the model-size sensitivity is system-dependent. We therefore obtained initial computational results from 4T and 28T structures for the protonated and sodiated ZSM-5 models for comparison.

For our larger calculations, a model representing the cavities of the MFI structure was constructed by initially extracting a 28T cluster from the literature crystal structure.[38] Dangling bonds were saturated with hydrogen atoms, with their locations obtained through optimizations with the PM6 semiempirical procedure, keeping the positions of the heavy atoms frozen. In subsequent calculations, the terminal hydrogen atoms were constrained in space to avoid unrealistic distortions of the model during the optimization procedure. ONIOM[39] calculations were carried out in which the clusters were partitioned into two layers, with atoms corresponding to the aluminum-containing active site belonging to the high-level layer. Geometry optimizations were carried out at the ONIOM-(BHandH-LYP/6-31+G(d,p):PM6) level, where the high-level atoms were optimized using BHandH-LYP/6-31+G(d,p) and the low-level atoms were optimized using the PM6 semiempirical procedure. Improved energies for all structures were obtained through calculations at the M06-2*X*/6-311+G(3df,2p) level.

For the smaller (4T) structures, geometries were optimized with the structures fully relaxed. Geometry optimizations for all structures were performed with BHandH-LYP/6-31+G(d,p) because it gives results comparable to B3-LYP (see the Supporting Information), which has been utilized in previous computational studies of zeolites with good effect,[40,41] but is better for some particularly flat potential energy surfaces. Improved energies for all structures were again obtained at the M06-2*X*/6-311+G(3df,2p) level.

Gibbs free energy corrections to 298 K, derived from the BHandH-LYP/6-31+G(d,p) calculations for the 4T structures and the ONIOM(BHandH-LYP/6-31+G(d,p):PM6) calculations for the 28T structures, were incorporated into the total energies. Literature scaling factors[42] were used in the evaluation of the Gibbs free energy corrections.

Comparison of the 4T and 28T results reveals that for the systems examined the free energy barriers of reaction are similar, even with different catalyst size (see the Supporting Information for details); therefore, 4T calculations were chosen for this study because a greater range of catalytic site models could be investigated with less demand on computational resources.

DOI: 10.1021/cs501677b
ACS Catal. 2015, 5, 4353−4362

Materials. The following chemicals were used as received: Ludox AS-40 (colloidal silica, 40 wt % in water), sodium aluminate ($NaAlO_2$), germanium(IV) oxide (GeO_2) (99.999%), tetraethyl orthosilicate (98%) (all Sigma-Aldrich), tetrapropylammonium hydroxide (TPAOH) (40 wt % in water) (Alfa Aesar) and glacial acetic acid (99.7%) (Ajax).

Zeolite Synthesis. A literature protocol was followed to prepare the Na-ZSM-5 and Na-Ge-ZSM-5 zeolites.[9] The Na-ZSM-5 and the Na-Ge-ZSM-5 samples were synthesized from mixtures with a molar composition of SiO_2/0.05$NaAlO_2$/0.27NaOH/0.21TPAOH/15H_2O/0.375AcOH and SiO_2/0.1GeO_2/0.05$NaAlO_2$/0.27NaOH/0.21TPAOH/15H_2O/0.375AcOH, respectively. In a typical synthesis of Ge-ZSM-5, 0.93 g of NaOH was dissolved in 9 mL of deionized water. To this mixture, 0.81 g of GeO_2 was added, and the mixture was stirred for 10 min to dissolve the GeO_2. An 11.42 g portion of Ludox AS-40 was added, and a white gel formed, which was stirred for 15 min. A separately prepared solution of 0.29 g of $NaAlO_2$ in 2.5 mL of deionized water was then added to the synthesis mixture. After 10 min of stirring, 8.0 g of TPAOH (40 wt % in water) was added dropwise, and the stirring was continued for 1.5 h. Using a solution of 1.8 g of glacial acetic acid in 5.4 mL of deionized water, the pH value was adjusted to around 10−11, and the solution was stirred for another 10 min. The synthesis mixture was transferred to a 50 mL PTFE-lined steel autoclave and heated to 160 °C over 72 h without stirring. The contents of the autoclave were centrifuged, and the isolated solid was washed three times with deionized water. The isolated material was dried at 80 °C, then calcined at 300 °C for 3 h, followed by 600 °C for 6 h (ramp rate, 1 °C/min). This material is denoted Na-Ge-ZSM-5. The germanium-free zeolite was synthesized following the same protocol (but without the addition of GeO_2) and is denoted Na-ZSM-5. For the aluminum-free germanium silicalite, a similar protocol was observed with the addition of GeO_2 retained but without the addition of $NaAlO_2$ to the reaction mixture. The material obtained is denoted Na-Ge-silicalite.

The K^+ or H^+ form of each zeolite was obtained after ion exchange by washing the zeolites three times in 50 mL KNO_3 or NH_3 (0.5 M) solution, respectively;[11] at room temperature; and sonicating for 5 min before centrifuging to isolate the solid, followed by washing the zeolite with deionized water each time. After drying at 80 °C, the zeolites were calcined at 280 °C for 3 h. The materials obtained are denoted K-Ge-ZSM-5, H-Ge-ZSM-5, and H-ZSM-5.

A procedure similar to that used for ion exchange was used for the removal of the amorphous germanate. The zeolite or silicalite was washed three times in 50 mL $NaNO_3$ solution (0.5 M) at room temperature[11] and sonicated for 5 min before centrifuging to isolate the solid, followed by washing the silicalite with deionized water each time. After drying at 80 °C, the silicalite was calcined at 280 °C for 3 h.

In a typical synthesis of silicalite,[43] 12.6 g of tetraethyl orthosilicate (TEOS), 20.0 g of TPAOH (1 M in water), and 0.7 g water were combined and stirred for 2 h. The mixture was transferred to an autoclave and heated at 160 °C for 48 h. The resulting silicalite is denoted H-silicalite. The Na^+ form of the silicalite was obtained after ion exchange by washing the silicalite three times in 50 mL $NaNO_3$ solution (0.5 M) at room temperature and sonicating for 5 min before centrifuging to isolate the solid, followed by washing the silicalite with deionized water each time. After drying at 80 °C, the silicalite was calcined at 280 °C for 3 h. The material obtained is denoted Na-silicalite.

For the sodium aluminogermanate synthesis, 0.51 g of NaOH was added to 7.3 mL of deionized water. To this solution, 4.1 g of GeO_2 was added, followed by 4.0 g of TPAOH dropwise, and the mixture was stirred overnight. In a separate flask, 0.15 g of $NaAl_2O_3$ was dissolved in 2 mL of deionized water, and this solution was added to the germanium mixture. The resulting mixture was stirred for 2 h, and the pH was then adjusted by adding 0.9 g of glacial acetic acid in 2.7 mL of deionized water. The gel was placed in a 25 mL PTFE-lined steel autoclave and heated to 160 °C for 72 h without stirring. The contents of the autoclave were centrifuged, and the solid was washed three times with deionized water. The isolated material was dried at 80 °C and then calcined at 300 °C for 3 h, followed by 600 °C for 6 h (ramp rate, 1 °C/min).

Characterization. Powder X-ray diffraction (XRD) measurements were made using a PANalytical X-Pert PRO MRD X-ray diffractometer equipped with a PIXcel detector and using Ni-filtered Cu Kα radiation (λ_{av}, 1.5419 Å). Initial analyses were performed using the PANalytical HighScore software. A Micromeritics ASAP 2020 Accelerated Surface Area and Porosity analyzer was used to measure the N_2 adsorption/desorption isotherms of the samples at 77 K. Before analysis, samples were degassed at 200 °C. Inductively coupled plasma−atomic emission spectroscopy (ICP−AES) was utilized to find the ratios of elements in the final products.

Catalytic Testing. As shown in Figure S4 (Supporting Information), the experimental setup comprises a coannular counter-current silica flow reactor housed vertically in a temperature-controlled furnace (Lindberg/Blue M 1100 °C, Moldatherm Box Furnace). Pure argon (100 sccm) controlled by a Smartrak mass flow controller (MFC) was bubbled through a 50% v/v aqueous solution of formic acid. Zeolite (150 mg) was fixed between two silica wool packages in a specific position at the lower end of the reaction tube (inside diameter, 0.7 cm). In a series of blank experiments, silica wool showed minimal decomposition of formic acid up to a temperature of 300 °C (Table 3). Two micro-GCs (Agilent micro-GC 4900) were used to sample the gaseous products at the outlet of the reactor. The GC columns used were a molecular sieve column (MS5A) for detecting hydrogen and carbon monoxide and a Pora-plot Q column (PPQ) for carbon dioxide. To protect the MS5A column from water vapor, the gaseous stream was dried by a Perma Pure Dryer (model PD 20−12 in.) before entering the GC.

■ ASSOCIATED CONTENT

Supporting Information

The Supporting Information is available free of charge on the ACS Publications website at DOI: 10.1021/cs501677b.

Comparison of results from B3-LYP and BHandH-LYP calculations. Comparison of results from 4T and 28T zeolite model structures. Full details of energies and energy corrections for all calculations. Details of formic acid complexes. Calculated IR and Raman spectra for zeolites with and without germanium. Details of 28T cluster structures utilized for the calculations. Time-on-stream data for Na-Ge-ZSM-5. XRD lattice constants for zeolites. Details of experiments to investigate mass-transfer limitations. Catalyst testing setup. Cartesian coordinates for all calculated molecules (PDF)

DOI: 10.1021/cs501677b
ACS Catal. 2015, 5, 4353−4362

AUTHOR INFORMATION

Corresponding Authors

*E-mail: ruth.amos@sydney.edu.au.
*E-mail: bun.chan@sydney.edu.au.
*E-mail: anthony.masters@sydney.edu.au.
*E-mail: thomas.maschmeyer@sydney.edu.au.
*E-mail: leo.radom@sydney.edu.au.

Notes

The authors declare no competing financial interest.

ACKNOWLEDGMENTS

We gratefully acknowledge funding (to C.J.E., T.M., A.M., and L.R.) from the Australian Research Council (ARC), funding (to R.I.J.A. and C.J.E) from the CSIRO, and generous grants of computer time (to L.R.) from the National Computational Infrastructure (NCI) National Facility and Intersect Australia Ltd. The authors thank Tom Savage and Elizabeth Carter for assistance with ICP–AES and Raman, respectively.

REFERENCES

(1) Epping Martin, K.; Kopasz, J. P.; McMurphy, K. W. In *Fuel Cell Chemistry and Operation*; Herring, A. M., Zawodzinski, T. A., Jr., Hamrock, S. J., Eds.; American Chemical Society: 2010; Vol. *1040*, p 1–13.
(2) Tedsree, K.; Li, T.; Jones, S.; Chan, C. W. A.; Yu, K. M. K.; Bagot, P. A. J.; Marquis, E. A.; Smith, G. D. W.; Tsang, S. C. E. *Nat. Nanotechnol.* **2011**, *6*, 302–307.
(3) Amos, R. I. J.; Heinroth, F.; Chan, B.; Zheng, S.; Haynes, B.; Easton, C.; Masters, A. F.; Radom, L.; Maschmeyer, T. *Angew. Chem., Int. Ed.* **2014**, *53*, 11275–11279.
(4) Cejka, J.; Centi, G.; Perez-Pariente, J.; Roth, W. J. *Catal. Today* **2012**, *179*, 2–15.
(5) Masters, A. F.; Maschmeyer, T. *Microporous Mesoporous Mater.* **2011**, *142*, 423–438.
(6) Abou-Kais, A.; Vedrine, J. C. *Chem. Phys. Lett.* **1977**, *45*, 117–120.
(7) Lefferts, L.; Seshan, K.; Mojet, B.; van Ommen, J. *Catal. Today* **2005**, *100*, 63–69.
(8) Kosslick, H.; Tuan, V. A.; Fricke, R.; Peuker, C. *Ber. Bunsen Ges. Phys. Chem.* **1992**, *96*, 1761–1765.
(9) Ghosh, A.; Vargas Garcia, N.; Mitchell, S. F.; Stevenson, S.; Shantz, D. F. *J. Phys. Chem. C* **2009**, *113*, 12252–12259.
(10) Van de Water, L. G. A.; Van der Waal, J. C.; Jansen, J. C.; Cadoni, M.; Marchese, L.; Maschmeyer, T. *J. Phys. Chem. B* **2003**, *107*, 10423–10430.
(11) Van de Water, L. G. A.; Van der Waal, J. C.; Jansen, J. C.; Maschmeyer, T. *J. Catal.* **2004**, *223*, 170–178.
(12) Lalik, E.; Liu, X.; Klinowski, J. *J. Phys. Chem.* **1992**, *96*, 805–809.
(13) Behrens, P.; Kosslick, H.; Vu, A. T.; Froeba, M.; Neissendorfer, F. *Microporous Mater.* **1995**, *3*, 433–441.
(14) Mentzel, U. V.; Hojholt, K. T.; Holm, M. S.; Fehrmann, R.; Beato, P. *Appl. Catal., A* **2012**, *417–418*, 290–297.
(15) Sauer, J. *J. Mol. Catal.* **1989**, *54*, 312–323.
(16) Lesthaeghe, D.; Van Speybroeck, V.; Waroquier, M. *Phys. Chem. Chem. Phys.* **2009**, *11*, 5222–5226.
(17) Sauer, J. *Stud. Surf. Sci. Catal.* **2007**, *172*, 19–26.
(18) Kosslick, H.; Tuan, V. A.; Fricke, R.; Peuker, C.; Pilz, W.; Storek, W. *J. Phys. Chem.* **1993**, *97*, 5678–5684.
(19) Chan, B.; Radom, L. *J. Am. Chem. Soc.* **2006**, *128*, 5322–5323.
(20) Malinowski, M.; Malinowska, K.; Zatorski, L. W. *Bull. Soc. Chim. Belg.* **1983**, *92*, 225–227.
(21) Frisch, M. J.; Trucks, G. W.; Schlegel, H. B.; Scuseria, G. E.; Robb, M. A.; Cheeseman, J. R.; Scalmani, G.; Barone, V.; Mennucci, B.; Petersson, G. A.; Nakatsuji, H.; Caricato, M.; Li, X.; Hratchian, H. P.; Izmaylov, A. F.; Bloino, J.; Zheng, G.; Sonnenberg, J. L.; Hada, M.; Ehara, M.; Toyota, K.; Fukuda, R.; Hasegawa, J.; Ishida, M.; Nakajima, T.; Honda, Y.; Kitao, O.; Nakai, H.; Vreven, T.; Montgomery, J. A., Jr.; Peralta, J. E.; Ogliaro, F.; Bearpark, M.; Heyd, J. J.; Brothers, E.; Kudin, K. N.; Staroverov, V. N.; Kobayashi, R.; Normand, J.; Raghavachari, K.; Rendell, A.; Burant, J. C.; Iyengar, S. S.; Tomasi, J.; Cossi, M.; Rega, N.; Millam, N. J.; Klene, M.; Knox, J. E.; Cross, J. B.; Bakken, V.; Adamo, C.; Jaramillo, J.; Gomperts, R.; Stratmann, R. E.; Yazyev, O.; Austin, A. J.; Cammi, R.; Pomelli, C.; Ochterski, J. W.; Martin, R. L.; Morokuma, K.; Zakrzewski, V. G.; Voth, G. A.; Salvador, P.; Dannenberg, J. J.; Dapprich, S.; Daniels, A. D.; Farkas, Ö.; Foresman, J. B.; Ortiz, J. V.; Cioslowski, J.; Fox, D. J. *Gaussian09*; Gaussian, Inc.: Wallingford CT, 2009.
(22) Chan, B.; Radom, L. *J. Am. Chem. Soc.* **2008**, *130*, 9790–9799.
(23) Hayashi, S.; Umemura, J.; Kato, S.; Morokuma, K. *J. Phys. Chem.* **1984**, *88*, 1330–1334.
(24) Marushkevich, K.; Khriachtchev, L.; Lundell, J.; Räsänen, M. *J. Am. Chem. Soc.* **2006**, *128*, 12060–12061.
(25) Chao, J.; Zwolinski, B. J. *J. Phys. Chem. Ref. Data* **1978**, *7*, 363–377.
(26) Miecznikowski, A.; Hanuza, J. *Zeolites* **1987**, *7*, 249–254.
(27) Nicolas, C. H.; Pera-Titus, M. *Microporous Mesoporous Mater.* **2012**, *153*, 254–262.
(28) Water could not be measured because of the aqueous reaction conditions but was assumed to be formed in a 1:1 ratio with CO, according to the dehydration mechanism shown in equation 2.
(29) Chopinet, M. H.; Fraissard, J. *Acta Phys. Chem.* **1978**, *24*, 107–112.
(30) Kamiya, K.; Tatsumi, M.; Matsuoka, J.; Nasu, H. *Phys. Chem. Glasses* **1998**, *39*, 9–16.
(31) Sierka, M.; Sauer, J. *Faraday Discuss.* **1997**, *106*, 41–62.
(32) Sauer, J.; Bleiber, A. *Catal. Today* **1988**, *3*, 485–92.
(33) Trzpit, M.; Soulard, M.; Patarin, J.; Desbiens, N.; Cailliez, F.; Boutin, A.; Demachy, I.; Fuchs, A. H. *Langmuir* **2007**, *23*, 10131–10139.
(34) Xiong, R.; Sandler, S. I.; Vlachos, D. G. *J. Phys. Chem. C* **2011**, *115*, 18659–18669.
(35) Bushuev, Y. G.; Sastre, G. *J. Phys. Chem. C* **2011**, *115*, 21942–21953.
(36) Kobayashi, T.; DiVerdi, J. A.; Maciel, G. E. *J. Phys. Chem. C* **2008**, *112*, 4315–4326.
(37) Van der Mynsbrugge, J.; De Ridder, J.; Hemelsoet, K.; Waroquier, M.; Van Speybroeck, V. *Chem. - Eur. J.* **2013**, *19*, 11568–11576.
(38) The ZSM-5 crystal structure was obtained from the Inorganic Crystal Structure Database (ICSD) and was originally published in Olson, D. H.; Kokotailo, G. T.; Lawton, S. L.; Meier, W. M. *J. Phys. Chem.* **1981**, *85*, 2238–2243.
(39) See for example: (a) Dapprich, S.; Komiromi, I.; Buyn, K. S.; Morokuma, K.; Frisch, M. J. *J. Mol. Struct.: THEOCHEM* **1999**, *461–462*, 1. (b) Vreven, T.; Byun, K. S.; Komaromi, I.; Dapprich, S.; Montgomery, J. A., Jr.; Morokuma, K.; Frisch, M. J. *J. Chem. Theory Comput.* **2006**, *2*, 815–826.
(40) Hemelsoet, K.; Lesthaeghe, D.; Van Speybroeck, V.; Waroquier, M. *J. Phys. Chem. C* **2007**, *111*, 3028–3037.
(41) Senger, S.; Radom, L. *J. Am. Chem. Soc.* **2000**, *122*, 2613–2620.
(42) Scott, A. P.; Radom, L. *J. Phys. Chem.* **1996**, *100*, 16502–16513.
(43) Kremer, S. P. B.; Kirschhock, C. E. A.; Aerts, A.; Villani, K.; Martens, J. A.; Lebedev, O. I.; Van Tendeloo, G. *Adv. Mater.* **2003**, *15*, 1705–1707.

DOI: 10.1021/cs501677b
ACS Catal. 2015, 5, 4353–4362